NHS Breast Screening Programme Equipment Report: Technical Evaluation of Fujifilm Sophinity digital mammography system in 2D mode

November 2025

Contents

Executive Summary

The technical performance of the Fujifilm Sophinity was assessed in 2D mode.

The Dance mean glandular dose (MGD) was found to be well below the remedial level for all automatic exposure control (AEC) dose modes. For a 53mm equivalent standard breast, the Dance MGD was 1.01mGy, compared with the remedial level of 2.5mGy. The image quality, measured by threshold gold thickness using the CDMAM 3.4 test object, was at the achievable level.

Technical performance of this equipment operating in 2D mode was found to be satisfactory and the system could proceed to practical evaluation of 2D mode. The technical evaluation of the performance in tomosynthesis mode will be published as a separate report.

Background

Mammographic equipment approved for use in the NHSBSP is subject to evaluation commissioned by NHS England and carried out by a number of breast screening services in England who undertake the practical evaluation of equipment using protocols provided by the NHSBSP. These evaluations comprise a staged process as follows:

1. A technical evaluation by the National Coordinating Centre for the Physics of Mammography ("NCCPM") (the "Technical Evaluation")

2. If the Technical Evaluation meets requirements, a subsequent practical evaluation is conducted by one of the breast screening services involved in the NHSBSP (the "Practical Evaluation")

Technical and Practical Evaluations are undertaken to assess the use of equipment in a practical, clinical setting and are not intended to be clinical trials. Further information about the limitations of the Technical Evaluation and Practical Evaluations are set out below.

The purpose of the Technical and Practical Evaluations together are intended to:

- determine the suitability of the equipment for use within the NHSBSP
- assist potential purchasers in making their choice of equipment
- provide potential users with performance data about equipment
- provide potential users with a record of the practical experience of using the equipment in the NHSBSP
- enable comparisons to be made with other pieces of tested equipment.

Disclaimer

Whilst NHS England commissions testing for the purposes outlined above, in order to provide further information and support to providers of screening services within the NHSBSP, it is for informational purposes only and such testing is subject to the limitations described below. No representation is made by NHS England in relation to the reports generated from the Technical Evaluation or the Practical Evaluation and, insofar as the law allows, NHS England accepts no liability arising from purchase or use of equipment by providers of screening services within the NHSBSP subjected to them.

Providers of screening services within the NHSBSP must ensure that all equipment purchased and used within the NHSBSP complies with all relevant requirements of the NHSBSP, the terms of their contracts in respect of the NHSBSP, and all other relevant obligations including but not limited to ensuring that such equipment:

- complies with national equipment standards
- has been approved for use in the programme and is tested by appropriately trained staff and medical physics services, in accordance with NHSBSP guidelines
- is accredited for use within the NHSBSP and that image quality and radiation dose meet acceptable standards
- is suitable for the usage intended in the breast screening unit.

Providers are reminded that they should carry out their own due diligence in respect of the above.

Testing undertaken during the Technical Evaluation is a balance between time, evaluation costs and depth. There are therefore limitations to the scope of the Evaluations undertaken on the behalf of the NHSBSP.

The Technical Evaluation is undertaken over a short time and so will not assess if image quality may change over time. The equipment tested is generally selected by the equipment supplier and has been set up by them. It should be noted that individual centres may be set up differently for example to meet the requirements of the screening service.

The technical image quality as measured on this system must be acceptable. The image quality of the final displayed image will be affected by the image processing and display and this is separately evaluated qualitatively in the Practical Evaluation.

This evaluation report does not absolve the provider of their responsibility during the procurement process to ensure the equipment is suitable for the usage intended by the provider.

1. Introduction

1.1 Testing procedures and performance standards for digital mammography

This report is one of a series evaluating commercially available direct digital radiography (DR) systems for mammography on behalf of the NHS Breast Screening Programme (NHSBSP) [1] [2] [3] [4]. The testing methods and standards applied are mainly derived from NHSBSP Equipment Report 0604 [5] which is referred to in this document as 'the NHSBSP protocol'. The standards for image quality and dose are the same as those provided in the European protocol [6] [7], but the latter has been followed where it provides a more detailed standard, for example, for the automatic exposure control (AEC) system.

Some additional tests were carried out according to the UK recommendations for testing mammography X-ray equipment as described in IPEM Report 89 [8].

1.2 Objectives

The aims of the evaluation were:

- to determine whether the Fujifilm Sophinity digital mammography system, operating in 2D mode, meets the main standards in the NHSBSP and European protocols
- to provide performance data for comparison against other systems.

2. Methods

2.1 System tested

The tests were conducted at the Fujifilm office in Bedford, England on a Fujifilm Sophinity system as described in Table 1. The Sophinity is shown in Figure 1.

Table 1. System description

Manufacturer	Fujifilm
Model	Sophinity
System serial number	JPH3353BTN
Target material	Tungsten (W)
Added filtration	50µm Rhodium (Rh) for 2D, 0.7mm Aluminium (Al) for tomosynthesis
Detector type	Amorphous selenium
Detector serial number	AC120251
Pixel pitch	50µm (The pixel matrix is hexagonal - the pixel pitch here is the resampled Cartesian pixel pitch in the final images)
Detector size	296.40 mm x 236.40 mm
Pixel array	5928 x 4728
Typical image sizes	32.78MB (237.0 mm x 177.0 mm field size) 54.75MB (296.4 mm x 236.4 mm field size)
Source to detector distance	650 mm
Source to table distance	640 mm
Pre-exposure mAs	mAs selection varies with CBT: 2 to 12mAs
Automatic exposure control (AEC) modes	iAEC on or off, ST (standard dose) or HQ (higher dose)
Software version	FDR-4000AWS Mainsoft V1.1.0001

The iAEC is an “intelligent” AEC system which segments pixels in the open field, implants, metal, and breast tissue. Using only the pixels identified as breast tissue the system estimates the glandular and adipose composition and selects appropriate exposure factors based on the estimated average density of the glandular tissue. Fujifilm recommend that iAEC is turned off for phantom exposures.

The pre-exposure factors for the AEC are selected according to the compressed breast thickness. These are calibrated for each system and may vary with x-ray tube age. The kV

selected for the final exposure can be changed by up to 2kV higher or lower than the pre-exposure and then the mAs calculated to get the signal required.

The system was tested using either manual factors or using settings of MAX4.0.

Figure 1. The Fujifilm Sophinity system (image supplied by Fujifilm)

2.2 Image processing

The Sophinity comes with default processing options corresponding to the manufacturers recommendations. The image processing is however customisable and typically applications specialists adjust contrast, edge enhancement, noise reduction etc. as requested by the customer. For these tests NCCPM left the processing unchanged from the machine defaults. Sites must be cautious if adjusting processing on any system and should involve

radiologists, medical physics experts and mammographers in a robust process to ensure that changes do not hide lesions or degrade reader performance.

2.3 Output and HVL

The output and half-value-layer (HVL) were measured as described in the NHSBSP protocol [6], at intervals of 3kV.

2.4 Detector response

The detector response was measured with 2mm thick aluminium at the tube head. The grid and paddle were removed and a dosimeter was positioned above the breast support, 50mm from the chest wall edge (CWE). The incident air kerma was measured for a range of manually set mAs values at 29kVp W/Rh anode/filter combination. The readings were corrected to the surface of the detector using the inverse square law. No correction was made for attenuation by the detector housing. A 10mm x 10mm region of interest (ROI) was positioned on the midline, 50mm from the CWE of each image. The average pixel value and the standard deviation of pixel values within the ROI were measured. The relationship between average pixel values and the incident air kerma to the detector was determined.

2.5 Dose estimation

Doses were measured by exposing different thicknesses of PMMA under AEC with both iAEC turned off and on. Each PMMA block had an area of 180mm x 240mm. The paddle height was set equal to the equivalent breast thickness, as shown in Table 3. The exposure factors were noted and mean glandular doses (MGDs) were calculated for breasts of equivalent thicknesses using the Dance dosimetry model [9] [10] [11].

Although not yet adopted in UK breast screening programmes, a joint AAPM TG282 and EFOMP report on breast dosimetry has been published [12]. The model proposed in this collaboration is intended by the authors as a future international standard. Mean glandular doses were therefore also estimated and tabulated using the TG282 model for cranio-caudal (CC) views applying TG282 median percentile glandularities. Software to perform the dose calculations can be downloaded from the AAPM, https://zenodo.org/records/10215098, and an online interface to the software is provided by NCCPM - TG282doseCalculator.

An aluminium square, 10mm x 10mm and 0.2mm thick, was used with the PMMA during these exposures, so that the images produced could be used for the calculation of the signal difference-to-noise ratio (SDNR), described in Section 2.6. The aluminium square was placed between two 10mm thick slabs of 180mm x 240mm PMMA, on the midline, with its

centre 50mm from the CWE. Additional layers of PMMA were placed on top to vary the total thickness.

2.6 Signal difference-to-noise ratio

Unprocessed images acquired during the dose measurement were analysed to obtain the SDNRs. Thirty six small square ROIs (approximately 2.5mm x 2.5mm) were used to determine the average signal and the standard deviation in the signal within the image of the aluminium square (4 ROIs) and the surrounding background (32 ROIs), as shown in Figure 2. Small ROIs are used to minimise distortions due to the heel effect and other causes of non-uniformity [13]. The SDNR was calculated for each image, as defined in the NHSBSP and European Protocols.

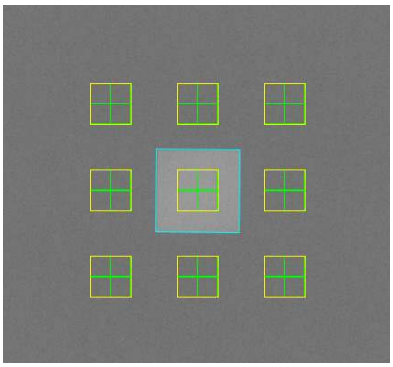

Figure 2: Location and size of ROI used to determine the SDNR

To apply the standards in the European protocol, it is necessary to relate the image quality measured using the CDMAM (Section 2.9) for an equivalent breast thickness of 60mm, to that for other breast thicknesses. The European protocol [7] gives the relationship between threshold contrast and SDNR measurements, enabling the calculation of a target SDNR value for a particular level of image quality. This can be compared to SDNR measurements made at other breast thicknesses. Contrast for a particular gold thickness is calculated using Equation 1, and target SDNR is calculated using Equation 2.

$$\text{Contrast} = 1 - e^{-\mu t} \quad (1)$$

where μ is the effective attenuation coefficient for gold, and t is the gold thickness.

$$SDNR_{target} = \frac{SDNR_{measured} \times TC_{measured}}{TC_{target}} \quad (2)$$

where $SDNR_{measured}$ is the SDNR for a 60mm equivalent breast, $TC_{measured}$ is the threshold contrast calculated using the threshold gold thickness for a 0.1mm diameter detail,

(measured using the CDMAM at the same dose as used for $SDNR_{measured}$), and TC_{target} is the calculated threshold contrast corresponding to the threshold gold thickness required to meet either the minimum acceptable or achievable level of image quality as defined in the NHSBSP protocol.

The threshold gold thickness for the 0.1mm diameter detail is used here because it is generally regarded as the most critical of the detail diameters for which performance standards are set.

The effective attenuation coefficient for gold used in Equation 1 depends on the beam quality used for the exposure, and the value used is in Table 2. This value was calculated with 3mm PMMA representing the compression paddle, using spectra from Hernandez et al [14] and attenuation coefficients for materials in the test objects (aluminium, gold, PMMA) from Berger et al [15].

The European protocol also defines a limiting value for SDNR, which is calculated as a percentage of the threshold contrast for minimum acceptable image quality for each thickness. This limiting value varies with thickness, as shown in Table 3.

Table 2. Effective attenuation coefficient for gold contrast details in the CDMAM

kVp	Target/filter	Effective attenuation coefficient (μm^{-1})
30	W/Rh	0.129

Table 3. Limiting values for relative SDNR

Thickness of PMMA (mm)	Equivalent breast thickness (mm)	Limiting values for relative SDNR (%) in European protocol
20	21	> 115
30	32	> 110
40	45	> 105
45	53	> 103
50	60	> 100
60	75	> 95
70	90	> 90

The target SDNR values for minimum acceptable and achievable levels of image quality and European limiting values for SDNR were calculated. These were compared with the measured SDNR results for all breast thicknesses.

2.7 AEC performance for local dense areas

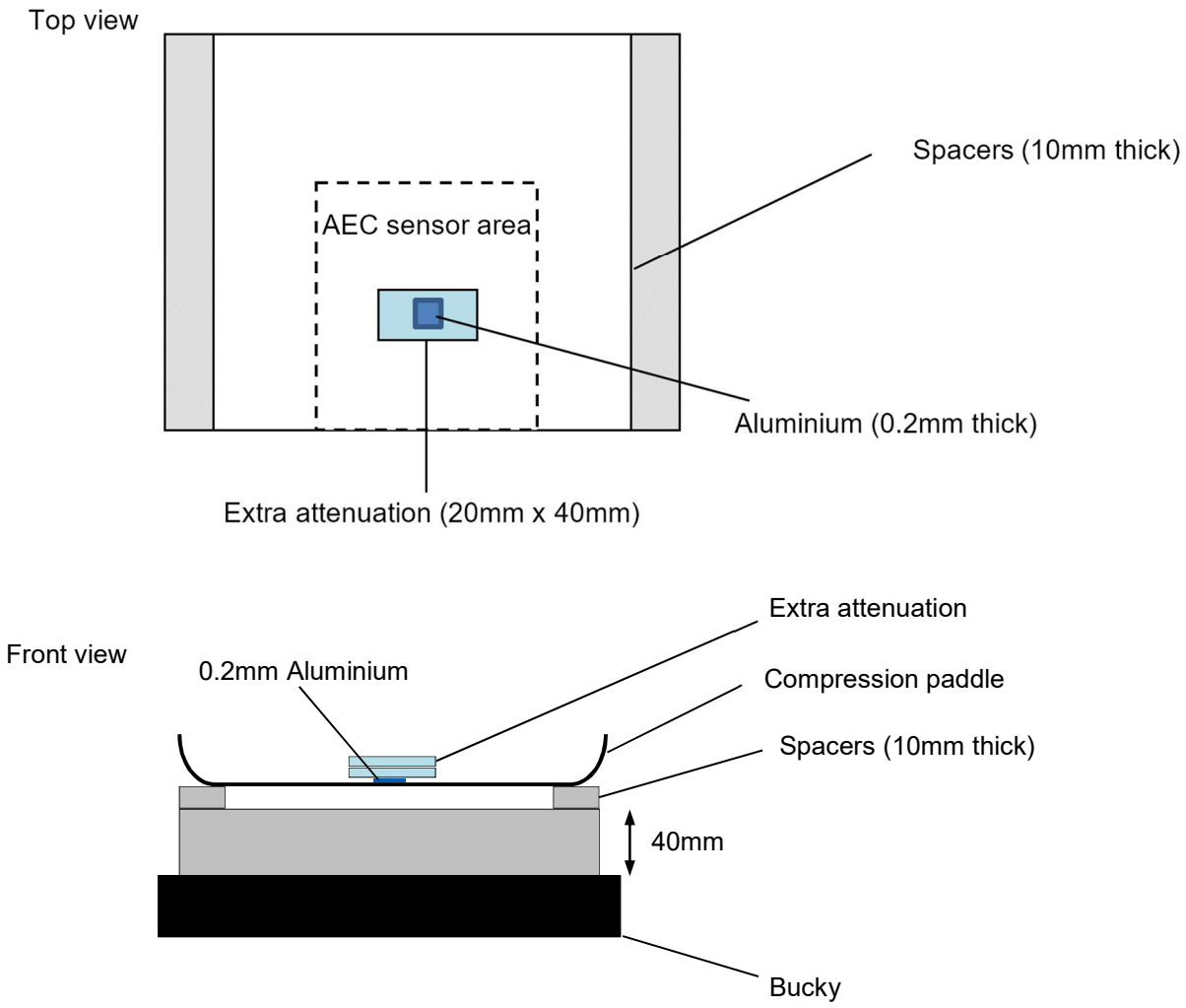

Figure 3. Setup to measure AEC performance for local dense areas

A test methodology for simulating local dense areas is described in the supplement to the fourth edition of the European protocol [7]. However, a more recent European protocol for DBT [16] includes some adaptions to the test which we believe to be equally useful in 2D mode. We have therefore implement these changes here. Images of a 40mm thick block of PMMA of size 180mm x 240mm, were acquired under AEC with a 50mm compression thickness. Additional pieces of PMMA of size 20mm x 40mm were added to provide extra attenuation of varying thicknesses in 4mm increments. An aluminium square, 10mm x 10mm

and 0.2mm thick was positioned centrally in the local dense region 50mm from the chest wall edge of the breast support table. The full test setup is shown in Figure 3.

In the simulated local dense area the mean pixel value and standard deviation for a 10mm x 10mm region of interest (ROI) were measured and the signal-to-noise ratios (SNRs) were calculated. ROIs of 5mm x 5mm were positioned over the aluminium and either side of it within the dense region. Each 5mm x 5mm ROI was subdivided into 1mm x 1mm elements. The mean pixel values and their standard deviations were averaged over all the 1mm x 1mm elements, and the SDNR was calculated from these averages.

2.8 Noise analysis

The images acquired in the measurements of detector response, using 29kVp W/Rh, were used to analyse the image noise. Small ROIs with an area of approximately 2.5mm x 2.5mm were placed on the midline, 50mm from the CWE. The average of the standard deviations of the pixel values in each of the ROIs for each image were used to investigate the relationship between the air kerma incident to the detector and the image noise. A power fit of standard deviation against incident air kerma was made. If electronic and structure noise are small then a square root relationship is expected. It was assumed that the noise in the image comprises three components: electronic noise, structural noise, and quantum noise. The relationship between them is shown in Equation 3:

$$\sigma_p = \sqrt{k_e^2 + k_q^2 p + k_s^2 p^2} \quad (3)$$

where σ_p is the standard deviation in pixel values within an ROI with a uniform exposure and a mean pixel value p, and k_e, k_q, and k_s are the coefficients determining the amount of electronic, quantum, and structural noise in a pixel with a value p. This method of analysis has been described previously [17]. For simplicity, the noise is generally presented here as relative noise defined as in Equation 4.

$$\text{Relative noise} = \sigma_p / p \quad (4)$$

The variation in relative noise with mean pixel value was evaluated and fitted using Equation 3, and non-linear regression used to determine the best fit for the constants and their asymptotic confidence limits. This established whether the experimental measurements of the noise fitted this equation, and the relative proportions of the different noise components. The relationship between noise and pixel values has been found empirically to be approximated by a simple power relationship as shown in Equation 5.

$$\sigma_p / p = k_t p^{-n} \quad (5)$$

where k_t is a constant. If the noise were purely quantum noise the value of n would be 0.5. However the presence of electronic and structural noise means that n can be slightly higher or lower than 0.5. For graphical presentation in this report pixel values were converted to incident air kerma at the detector using the detector response data described in section 2.3.

The variance in pixel values within a ROI is defined as the standard deviation squared. The total variance against incident air kerma at the detector was fitted using Equation 3. Non-linear regression was used to determine the best fit for the constants and their asymptotic confidence limits.

Using the calculated constants, the structural, electronic, and quantum components of the variance were estimated, assuming that each component was independently related to incident air kerma. The percentage of the total variance represented by each component was then calculated and plotted against incident air kerma at the detector.

2.9 Image quality measurements

Contrast detail measurements were made using a CDMAM phantom (serial number 1022, version 3.4, UMC St. Radboud, Nijmegen University, Netherlands). The phantom was positioned with a 20mm thickness of PMMA above and below, to give a total attenuation approximately equivalent to 50mm of PMMA or 60mm thickness of typical breast tissue. The exposure factors were chosen to match as closely as possible those selected by the AEC, at the standard dose setting, when imaging a 50mm thickness of PMMA. This procedure was repeated to obtain a representative sample of 16 images at this dose level. Further sets of 16 images of the test phantom were then obtained at other dose levels by manually selecting higher and lower mAs values with the same beam quality.

The CDMAM images were read and analysed automatically using Version 1.6 of CDCOM [18] [19]. and Version 2.1.0 of CDMAM Analysis (https://medphys.royalsurrey.nhs.uk/nccpm/). The threshold gold thickness for a typical human observer was predicted using Equation 6.

$$TC_{predicted} = rTC_{auto} \quad (6)$$

where $TC_{predicted}$ is the predicted threshold contrast for a typical observer, TC_{auto} is the threshold contrast measured using an automated procedure with CDMAM images. r is the average ratio between human and automatic threshold contrast determined experimentally with the values shown in Table 4.

The process was repeated using a CDMAM 4.0 phantom (serial number 4306, version 4.0, UMC St. Radboud, Nijmegen University, Netherlands).

Table 4. Values or r used to predict threshold contrast

Diameter of gold disc (mm)	Average ratio of human to automatically measured threshold contrast (r)
0.08	1.40
0.10	1.50
0.13	1.60
0.16	1.68
0.20	1.75
0.25	1.82
0.31	1.88
0.40	1.94
0.50	1.98
0.63	2.01
0.80	2.06
1.00	2.11

The predicted threshold gold thickness for each detail diameter in the range 0.1mm to 1.0mm was fitted with a curve for each dose level, using the relationship shown in Equation 7.

$$\text{Threshold gold thickness} = a + bx^{-1} + cx^{-2} + dx^{-3} \quad (7)$$

where x is the detail diameter, and a, b, c and d are coefficients adjusted to obtain a least squares fit.

The confidence limits for the predicted threshold gold thicknesses have been previously determined by a sampling method using a large set of images. The threshold contrasts quoted in the tables of results are derived from the fitted curves.

The expected relationship between threshold contrast and MGD is shown in Equation 8.

$$\text{Threshold contrast} = \lambda D^{-n} \quad (8)$$

where D is the MGD for a 60mm thick standard breast (equivalent to the test phantom configuration used for the image quality measurement), and λ is a constant to be fitted.

It is assumed that a similar equation applies when using threshold gold thickness instead of contrast. This equation was plotted with the experimental data for detail diameters of 0.1 and 0.25mm. The value of n resulting in the best fit to the experimental data was determined, and the doses required for target SDNR values were calculated for data relating to these detail diameters.

The MGDs to reach the minimum and achievable image quality standards in the NHSBSP protocol were then estimated. The error in estimating these doses depends on the accuracy of the curve fitting procedure, and pooled data for several systems has been used to estimate 95% confidence limits of about 20%.

2.10 Physical measurements of the detector performance

The modulation transfer function (MTF), normalised noise power spectrum (NNPS) and the detective quantum efficiency (DQE) of the system were measured. The methods used were as close as possible to those described by the International Electrotechnical Commission (IEC) [20]. The radiation quality used for the measurements was adjusted by placing a uniform 2mm thick aluminium filter at the tube housing. The beam quality used was 29kVp W/Rh. The test device to measure the MTF comprised a 120mm x 60mm rectangle of stainless steel with a polished straight edge, of thickness 2mm. This test device was placed directly on the breast support table, and the grid was removed. The test device was positioned to measure the MTF in two directions, first almost perpendicular to the CWE and then almost parallel to it.

To measure the noise power spectrum the test device was removed and exposures made for a range of incident air kerma at the surface of the table. The DQE is presented as the average of measurements in the directions perpendicular and parallel to the CWE.

2.11 Projection function (positioning MAP) and positioning analysis

Fujifilm Sophinity features a projection function in which the breast outline from prior mammograms can be projected onto the breast support. This is intended to aid positioning and consistency of positioning between rounds. Fujifilm recommend that mammographers always strive to provide better coverage than the previous mammograms but as an absolute minimum match the past coverage. In addition, Fujifilm provide an optional AI based positioning analysis tool that provides feedback on the quality of the mammographic positioning.

The tests that could be performed on these functions without a real client were limited. An anatomical phantom was imaged and the examination completed without moving the

phantom. A new patient study was created and the alignment of the projection outline was compared visually against the true phantom edge which had remained fixed. This process was repeated for a few different positions of the phantom.

2.12 Other tests

Other tests carried out included tests prescribed in IPEM Report 89 [8] for mammographic X-ray sets, as well as those in the NHSBSP protocol for digital mammographic systems. In addition to the five ROI method for uniformity described in these documents, uniformity was also assessed using a sliding ROI of size 2mm by 2mm.

3. Results

3.1 Output and HVL

The output and HVL measurements are shown in Table 5.

Table 5. Output and HVL

kVp	Target/filter	Output (μGy/mAs at 1m)	HVL (mm Al)
22	W/Rh	6.4	0.44
25	W/Rh	10.7	0.49
28	W/Rh	14.8	0.54
31	W/Rh	18.9	0.57
34	W/Rh	23.0	0.60
37	W/Rh	27.0	0.63
40	W/Rh	31.0	0.64

3.2 Detector response

The detector response is shown in Figure 4.

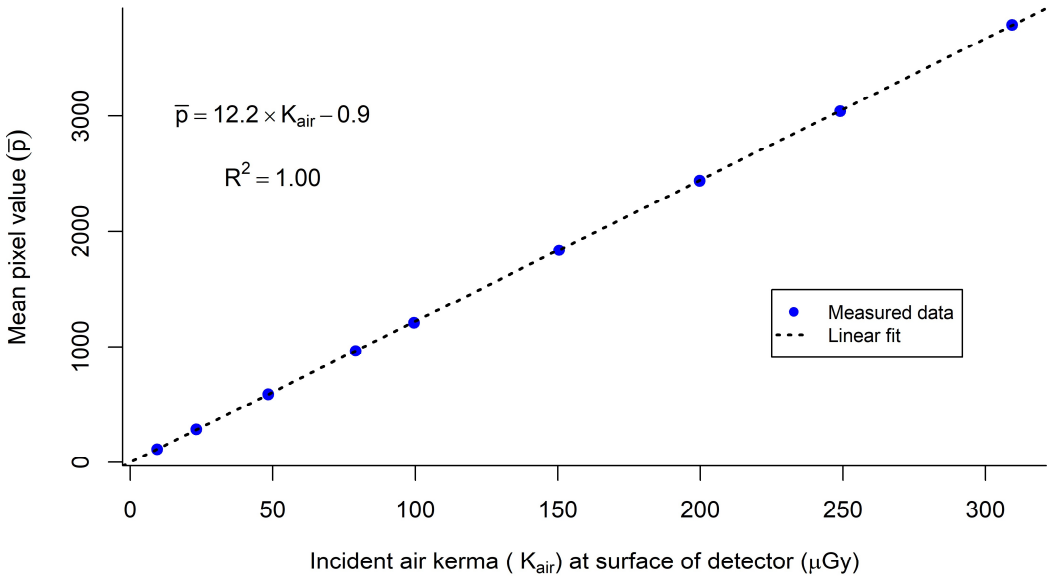

Figure 4. Detector response acquired at 29kVp W/Rh anode/filter combination with 2mm Al at the tube port

3.3 AEC performance

3.3.1 Dose

The MGDs for breasts simulated with PMMA exposed under AEC control are shown in Table 6 for exposures made in ST mode and in table 7 for exposures made in HQ mode. The mAs values in all tables are the displayed figures and exclude the pre-exposure. The MGDs were calculated including the contribution from the pre-exposure which was calculated using the pre-exposure kVp, tube current and exposure time. The factors of each individual shot can be found on the AWS information button for each exposure, they are not stored in the DICOM headers. The values used for these measurements are shown in Table 8. It can be seen that the kV sometimes changed between the pre-exposure and the final exposure. The results presented in Table 6 and Table 7 are also presented graphically in Figure 5.

Table 6. MGD for simulated breasts (ST mode)

		iAEC on				iAEC off			
Equivalent breast thickness (mm)	kVp	mAs	Dance MGD (mGy)	TG282 MGD (mGy)	Displayed dose (mGy)	mAs	Dance MGD (mGy)	TG282 MGD (mGy)	Displayed dose (mGy)
21	26	31.3	0.52	0.53	0.52	30.3	0.51	0.52	0.50
32	27	45.5	0.69	0.70	0.69	44.1	0.67	0.68	0.66
45	28	60.7	0.89	0.84	0.88	59.6	0.87	0.83	0.86
53	29	69.0	1.03	0.92	1.05	67.4	1.01	0.90	1.02
60	30	83.5	1.28	1.07	1.31	81.9	1.26	1.05	1.28
75	31	112.0	1.68	1.20	1.73	108.0	1.62	1.16	1.67
90	33	147.5	2.26	1.44	2.41	139.5	2.15	1.36	2.27
103	34	199.9	2.99	1.73	3.23	190.1	2.85	1.65	3.07

Table 7. MGD for simulated breasts (HQ mode)

		iAEC on				iAEC off			
Equivalent breast thickness (mm)	kVp	mAs	Dance MGD (mGy)	TG282 MGD (mGy)	Displayed dose (mGy)	mAs	Dance MGD (mGy)	TG282 MGD (mGy)	Displayed dose (mGy)

21	26	46.6	0.76	0.78	0.78	44.9	0.73	0.75	0.75
32	27	68.3	1.01	1.03	1.03	65.8	0.98	0.99	0.99
45	28	89.2	1.27	1.21	1.30	87.4	1.25	1.18	1.27
53	29	102.0	1.49	1.33	1.55	99.3	1.45	1.29	1.51
60	30	123.1	1.85	1.55	1.93	120.2	1.81	1.52	1.88
75	31	166.4	2.44	1.75	2.57	160.2	2.35	1.69	2.48
90	33	217.6	3.28	2.08	3.55	205.1	3.10	1.97	3.35
103	34	296.8	4.36	2.51	4.80	280.2	4.13	2.38	4.53

Table 8. Pre-exposure factors (W/Rh anode/filter)

Equivalent breast thickness (mm)	kVp	mAs	Dance MGD (mGy)	TG282 MGD (mGy)
21	27	1.55	0.03	0.028
32	28	2.31	0.04	0.028
45	28	4.44	0.06	0.038
53	29	4.93	0.07	0.057
60	30	5.19	0.08	0.061
75	31	7.55	0.11	0.063
90	33	8.61	0.12	0.076
103	35	10.97	0.17	0.079

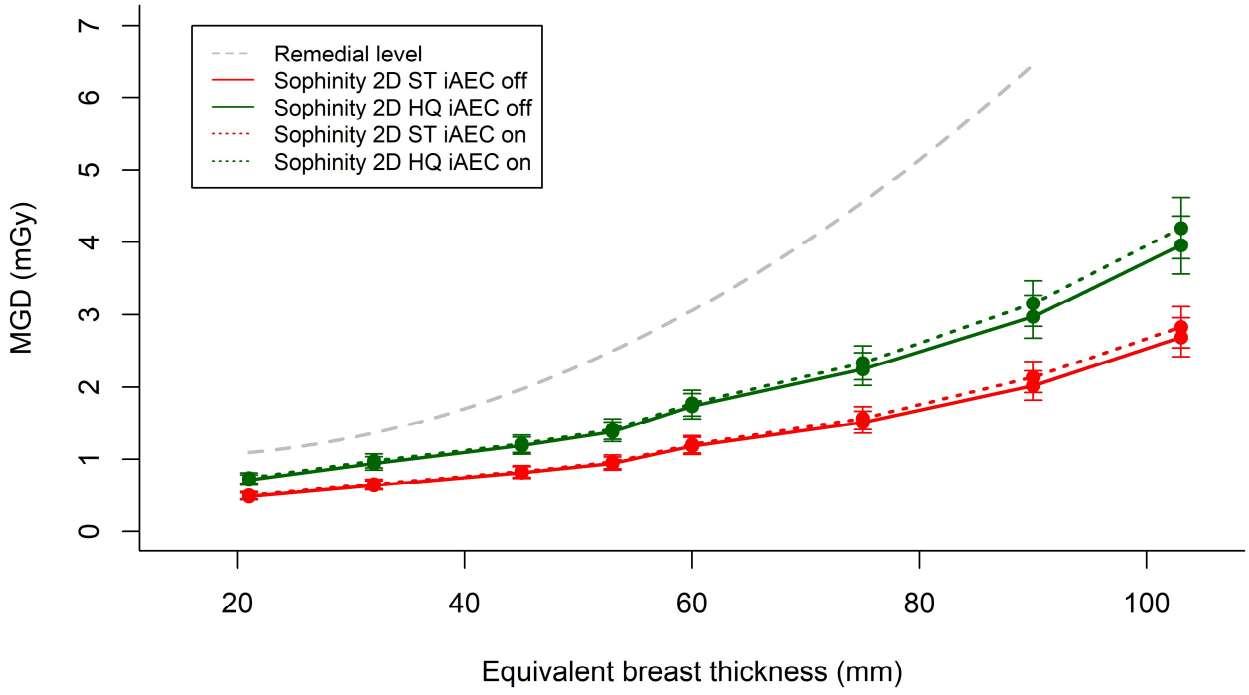

Figure 5. Dance MGD for different thicknesses of simulated breasts (Error bars indicate 95% confidence limits

3.3.2 Signal difference-to-Noise ratio

The results of the SDNR measurements for images acquired in ST mode and HQ mode are shown in tables 8 and 9 respectively and in Figure 6. The following calculated values are also shown:

- SDNR to meet the minimum acceptable image quality standard
- SDNR to meet the achievable image quality standard
- SDNRs at each thickness to meet the limiting value in the European protocol

Table 9. SDNR measurements (ST mode)

PMMA (mm)	Equivalent breast thickness (mm)	Measured SDNR (iAEC off)	Measured SDNR (iAEC on)	SDNR for minimum acceptable IQ	SDNR for achievable IQ	European limiting SDNR value
20	21	8.6	8.7	3.9	5.8	4.5
30	32	7.5	7.7	3.9	5.8	4.3
40	45	6.5	6.5	3.9	5.8	4.1
45	53	6.0	6.2	3.9	5.8	4.1
50	60	5.8	5.9	3.9	5.8	3.9
60	75	4.9	5.0	3.9	5.8	3.7
70	90	4.1	4.3	3.9	5.8	3.5

Table 10. SDNR measurements (HQ mode)

PMMA (mm)	Equivalent breast thickness (mm)	Measured SDNR (iAEC off)	Measured SDNR (iAEC on)	SDNR for minimum acceptable IQ	SDNR for achievable IQ	European limiting SDNR value
20	21	10.5	10.7	3.9	5.8	4.5
30	32	9.2	9.2	3.9	5.8	4.3
40	45	7.9	8.0	3.9	5.8	4.1
45	53	7.3	7.5	3.9	5.8	4.1
50	60	7.1	7.1	3.9	5.8	3.9
60	75	6.0	6.2	3.9	5.8	3.7
70	90	5.1	5.2	3.9	5.8	3.5

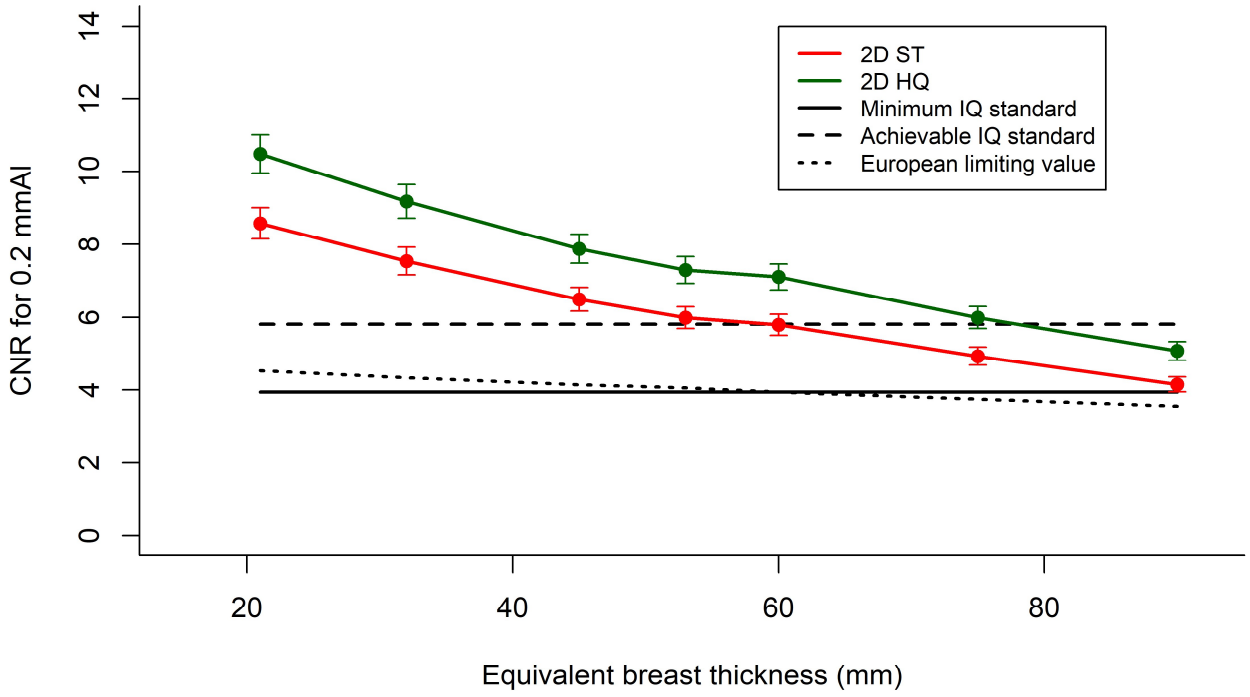

Figure 6. Measured SDNR compared with the limiting values in the European protocol. (Error bars indicate 95% confidence limits.)

3.3.3 AEC performance for local dense areas

In grid mode it is expected that when the AEC adjusts for local dense areas, the SNR and SDNR remain constant with increasing thickness of extra PMMA. The results presented in Tables 11 and 12, Figures 7 and 8 show that the SNR and SDNR do remain fairly constant as thickness increases up to a total attenuation of 52mm PMMA.

Table 11. AEC performance for local dense areas iAEC off

Total attenuation (mm PMMA)	Target / filter	kVp	Tube load (mAs)	SDNR	SDNR deviation (%)	SNR	% SNR difference from mean SNR result	MGD (mGy)	MGD deviation (%)
40	W/Rh	28	54.9	6.0	1.3	42.8	1.9	0.76	-18.1
44	W/Rh	28	68.1	6.0	0.0	41.9	-0.3	0.93	0.0
48	W/Rh	28	84.8	5.9	-0.4	41.7	-0.7	1.14	22.9
52	W/Rh	29	93.8	5.8	-2.5	41.7	-0.8	1.33	43.0

Table 12. AEC performance for local dense areas iAEC on

Total attenuation (mm PMMA)	Target / filter	kVp	Tube load (mAs)	SDNR	SDNR deviation (%)	SNR	% SNR difference from mean SNR result	MGD (mGy)	MGD deviation (%)
40	W/Rh	28	56.8	6.1	0.1	43.1	0.9	0.79	-18.0
44	W/Rh	28	70.3	6.1	0.0	43.0	0.6	0.96	0.0
48	W/Rh	29	77.7	5.9	-4.2	42.8	0.0	1.16	21.5
52	W/Rh	29	95.7	5.8	-4.7	42.1	-1.5	1.42	48.2

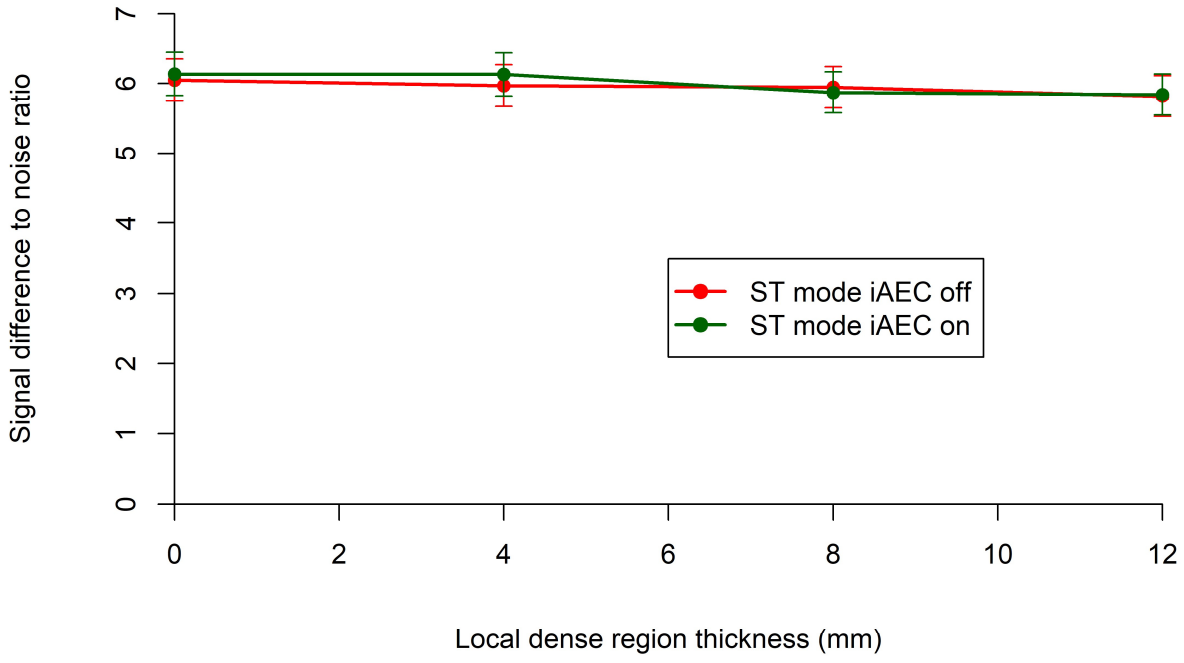

Figure 7. AEC performance for local dense areas (signal difference to noise ratio)

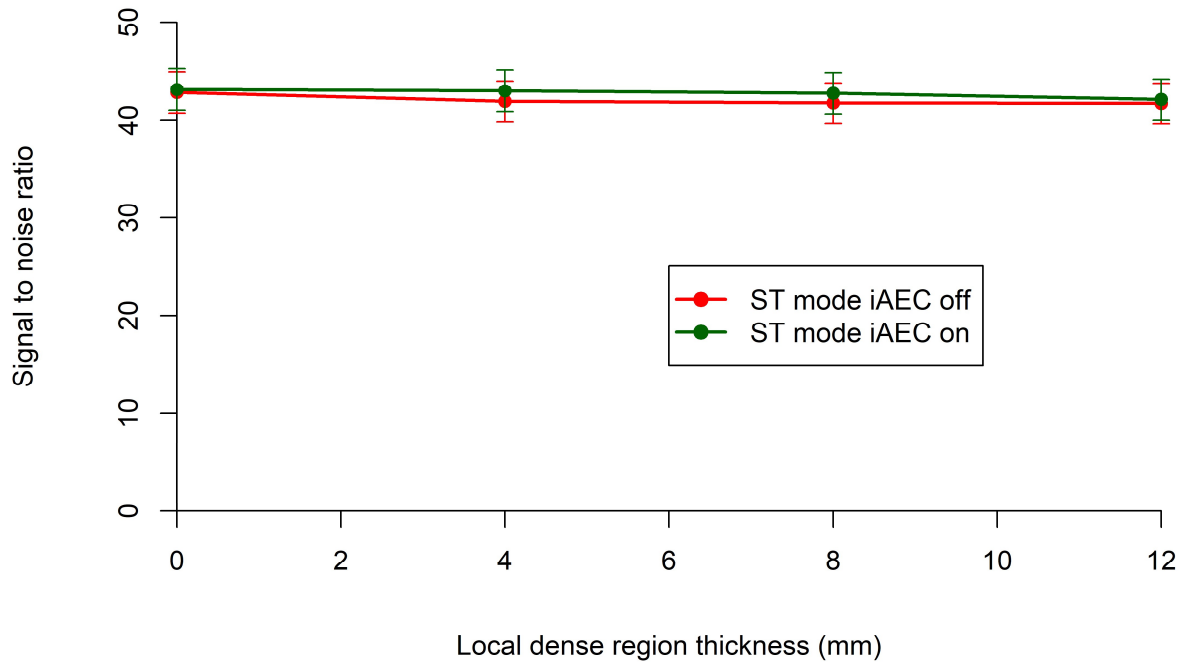

Figure 8. AEC performance for local dense areas (signal to noise ratio)

3.4 Noise measurements

The variation in noise with dose was analysed by plotting the standard deviation in pixel values against the incident air kerma to the detector, as shown in Figure 9. The fitted power curve has an index of 0.48, which is close to the expected value of 0.5 for quantum noise sources alone.

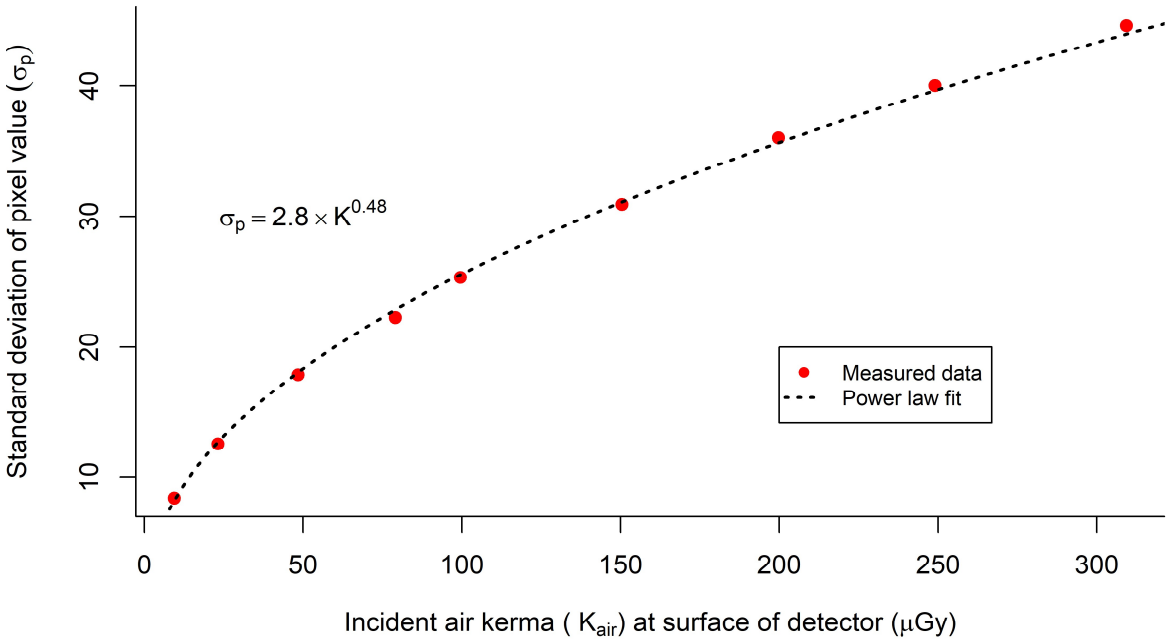

Figure 9. Standard deviation of linearized pixel values versus incident air kerma at detector

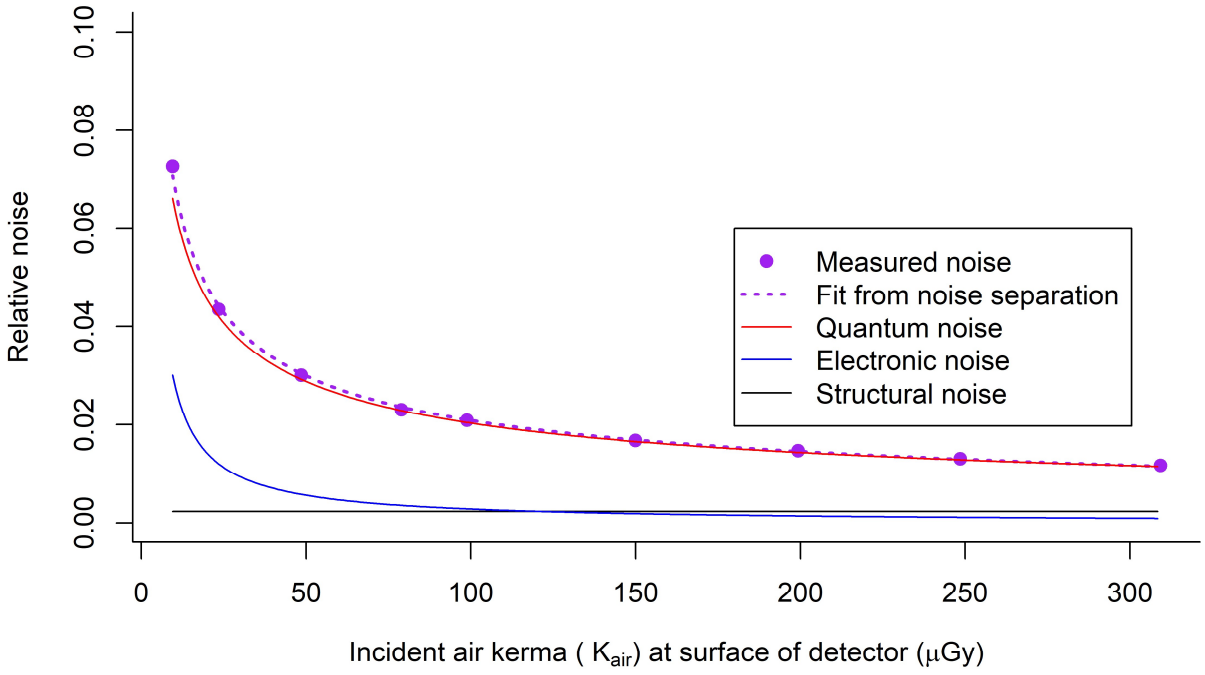

Figure 10. Relative noise and noise components

Figure 10 shows the relative noise at different incident air kerma. The estimated relative contributions of electronic, structural, and quantum noise are shown and the quadratic sum of these contributions fitted to the measured noise (using Equation 3).

Figure 11 shows the different amounts of variance due to each component. From this, the dose range over which the quantum component dominates can be seen.

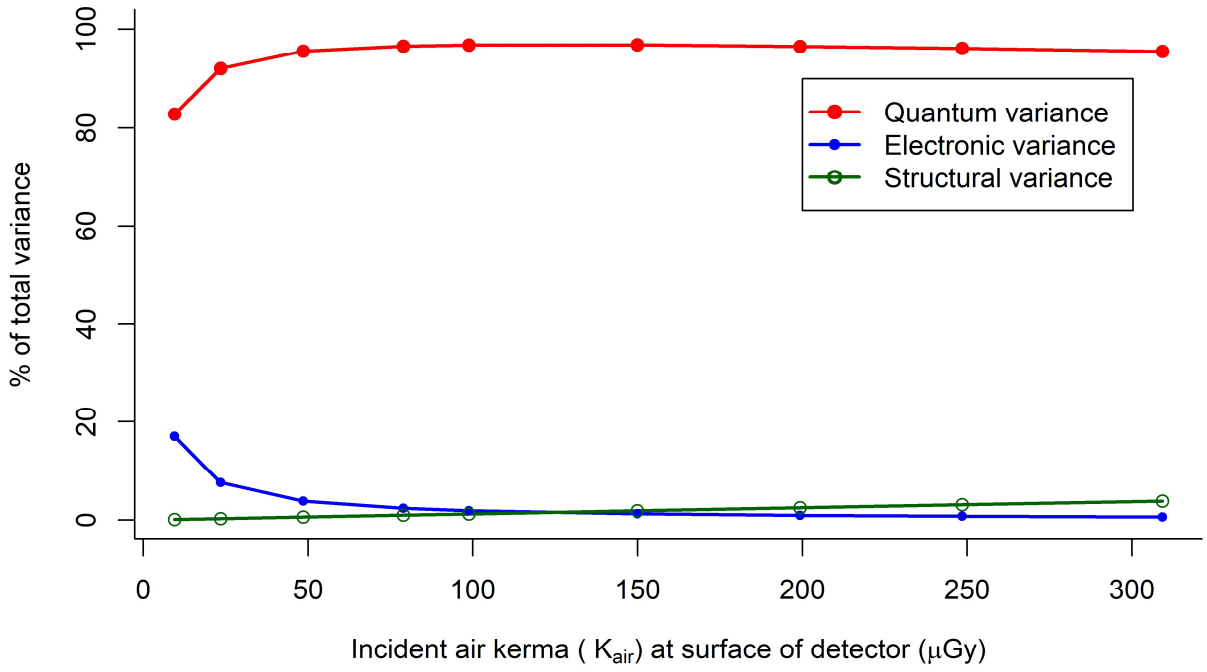

Figure 11. Noise components as a percentage of the total variance

3.5 Image quality measurements

The exposure factors used for each set of 16 CDMAM images are shown in Table 12 excluding the pre-pulse. The Dance MGDs ranged from half to two times the dose of 1.15mGy, which was close to that selected for the equivalent breast of 60mm thick in AEC mode.

Table 13. Images acquired for image quality measurement

kVp	Target/filter	Tube loading (mAs)	Mean glandular dose to equivalent breasts 60mm thick (mGy)
30	W/Rh	36.0 (0.45x AEC ST)	0.52
30	W/Rh	56.0 (0.7x AEC)	0.81
30	W/Rh	80.0 (1.0x AEC ST)	1.15
30	W/Rh	123.0 (1.0x AEC HQ)	1.77
30	W/Rh	178.0 (2.2x AEC ST)	2.56

The contrast detail curves (determined by automatic reading of the images) at the different dose levels are shown in Figure 12. The threshold gold thicknesses measured for different detail diameters at the 5 selected dose levels are shown in Table 13. The NHSBSP minimum acceptable and achievable limits are also shown.

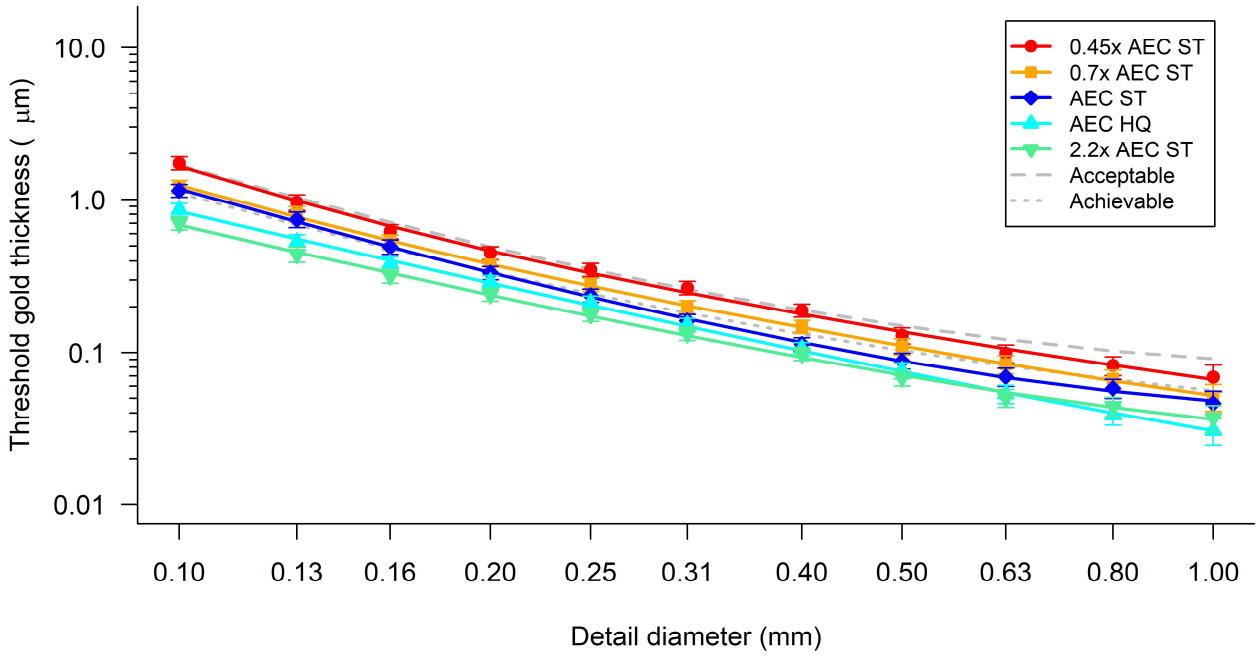

Figure 12. Threshold gold thickness detection curves for 5 doses at 30kV W/Rh (Error bars indicate 95% confidence limits.) – CDMAM3.4

Table 14. Average threshold gold thicknesses for different detail diameters for 5 doses using 30kVp W/Rh, and automatically predicted data – CDMAM 3.4

Diam-eter (mm)	Accept-able value	Achiev-able value	Threshold gold thickness (µm) Mean Glandular Dose to equivalent breast 60mm thick (mGy)				
			0.52	0.81	1.15	1.77	2.56
0.1	1.68	1.1	1.65 ± 0.17	1.24 ± 0.12	1.17 ± 0.11	0.84 ± 0.08	0.69 ± 0.07
0.25	0.352	0.244	0.33 ± 0.04	0.27 ± 0.03	0.23 ± 0.02	0.20 ± 0.02	0.17 ± 0.02
0.5	0.15	0.103	0.14 ± 0.02	0.11 ± 0.01	0.09 ± 0.01	0.08 ± 0.01	0.07 ± 0.01
1	0.091	0.056	0.07 ± 0.01	0.05 ± 0.01	0.05 ± 0.01	0.03 ± 0.01	0.04 ± 0.01

The measured threshold gold thicknesses are plotted against the Dance MGD for an equivalent breast for the 0.1mm and 0.25mm detail sizes in Figure 14 from Table 13.

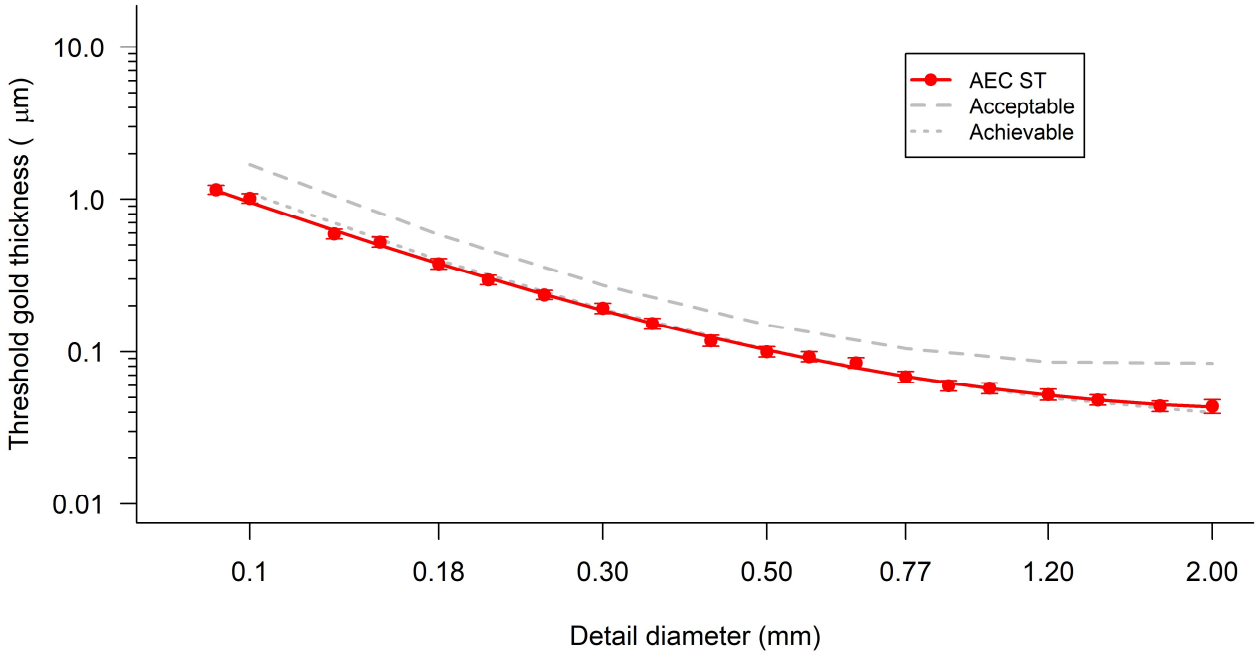

Figure 13. Threshold gold thickness detection curves for AEC dose setting at 30kV W/Rh (Error bars indicate 95% confidence limits) - CDMAM4.0

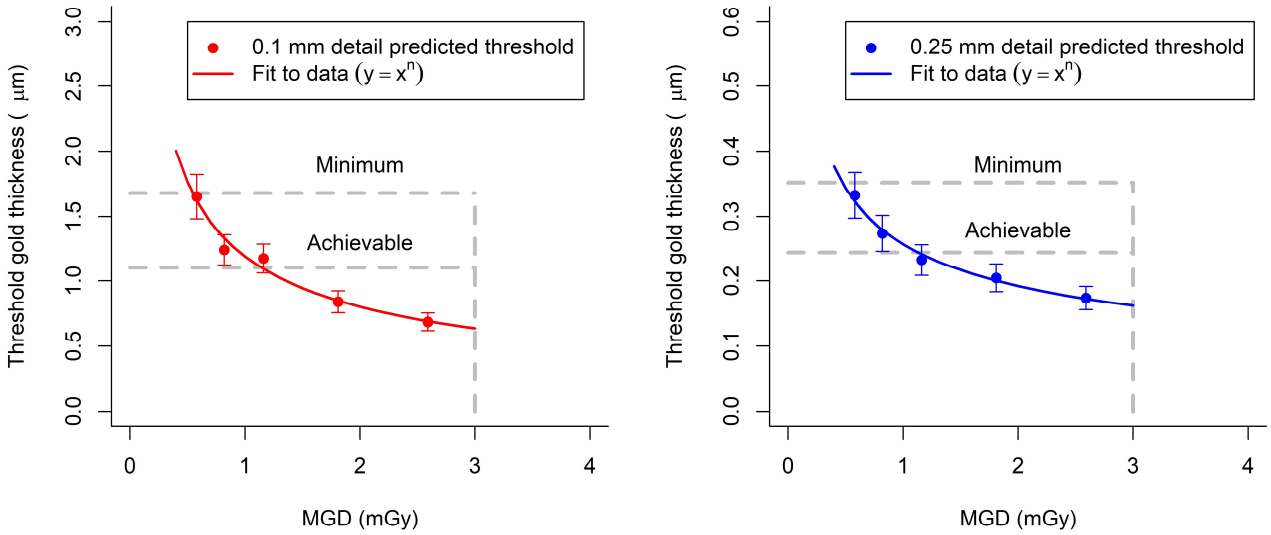

Figure 14. Threshold gold thickness at different doses. (Error bars indicate 95% confidence limits)

The Dance MGDs to reach the minimum and achievable image quality standards in the NHSBSP protocol for a 60mm equivalent breast thickness have been estimated from the curves shown in Figure 14. To reach the minimum threshold gold thickness Dance MGDs of 0.55 ± 0.11 mGy and 0.48 ± 0.10 mGy were required for 0.1 mm and 0.25mm details respectively. To reach the achievable threshold gold thickness Dance MGDs of 1.15 ± 0.23 mGy and 1.13 ± 0.23 mGy were required for 0.1mm and 0.25mm details respectively.

3.6 Quantitative measurements

The MTF is shown in Figure 15 for the two orthogonal directions. Figure 16 shows the NNPS curves for a range of air kerma incident to the detector. These are measured in the system

and so the results will be influenced not only by the detector but the system.

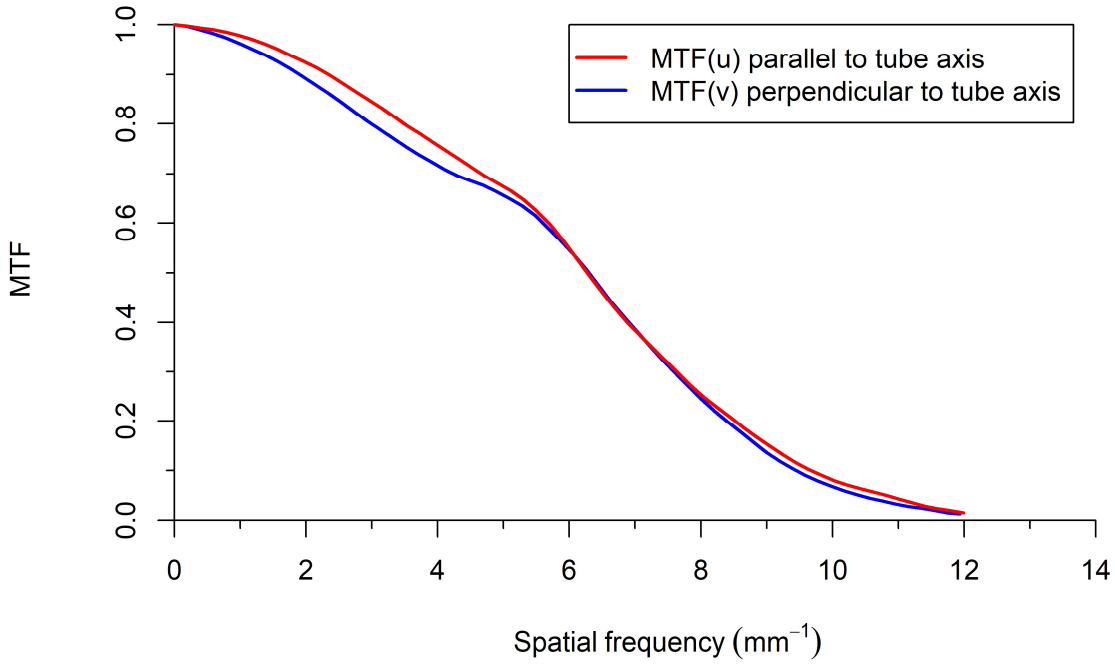

Figure 15. Pre-sampled MTF

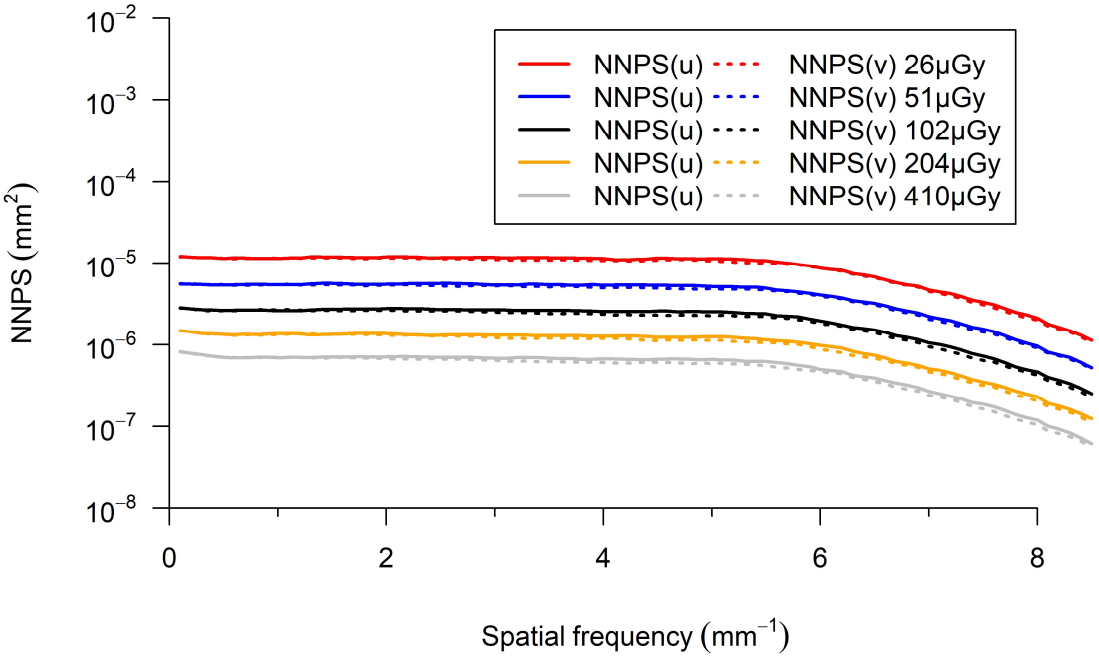

Figure 16. NNPS curves for a range of air kerma incident to the detector

Figure 17 shows the DQE averaged in two orthogonal directions for a range of incident air kerma. The values are truncated at the Nyquist frequency. This was calculated using the approach of Aiazzi et al. [21] from the underlying hexagonal pixel spacing, rather than the resampled image grid. The spectra of Hernandez et al [14] were attenuated using the Bier-Lambert law with mass attenuation coefficients from Berger et al [15] and the mammographic filter thickness was adjusted iteratively until the calculated HVL matched the results in Table 5. The resulting spectra were used to estimate a *q*-factor of 6173 photons mm^{-2} μGy^{-1}. The MTF and DQE measurements were interpolated to show values at standard frequencies in Table 14.

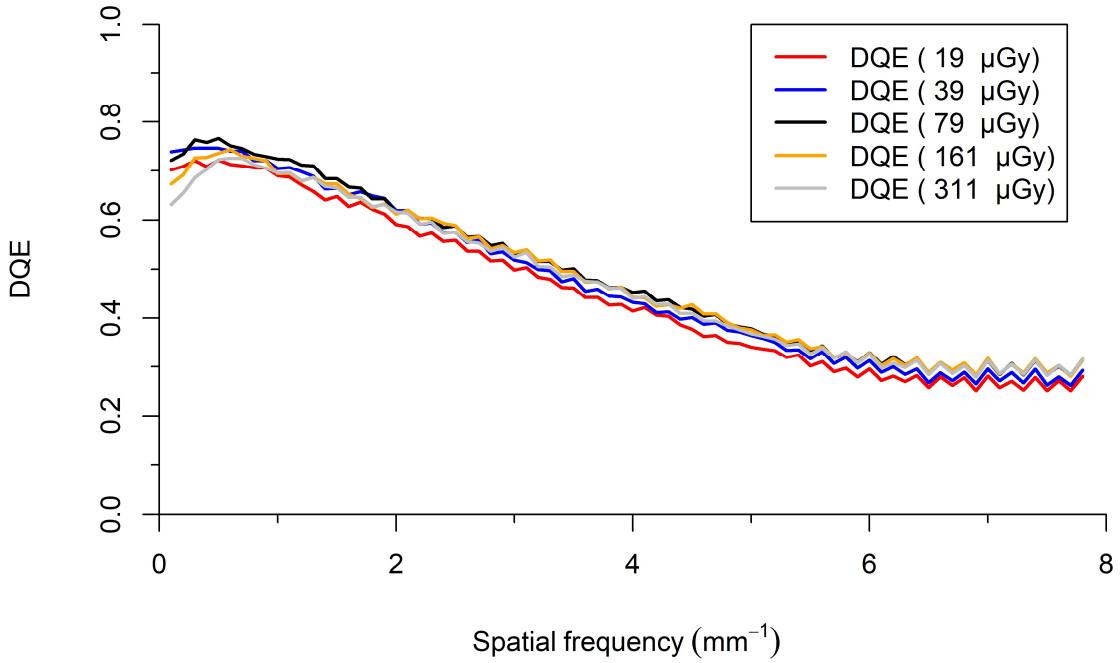

Figure 17. DQE averaged in both directions for a range of incident air kerma

Table 15. MTF and DQE measurements at standard frequencies (DQE at incident air kerma of 102µGy)

Frequency (mm^{-1})	MTF(u)	MTF(v)	DQE	Frequency (mm^{-1})	MTF(u)	MTF(v)	DQE
0.0	1.00	1.00	-	4.5	0.72	0.69	0.41
0.5	0.99	0.99	0.77	5.0	0.67	0.66	0.38
1.0	0.97	0.96	0.72	5.5	0.62	0.60	0.34
1.5	0.96	0.93	0.68	6.0	0.55	0.55	0.33
2.0	0.92	0.89	0.62	6.5	0.45	0.46	0.28
2.5	0.89	0.85	0.59	7.0	0.39	0.39	0.31
3.0	0.84	0.80	0.53	7.5	0.31	0.31	0.28
3.5	0.80	0.76	0.50	8.0	0.26	0.26	0.30
4.0	0.75	0.72	0.45				

3.7 Projection function (positioning MAP)

The system successfully identified the breast edge in the prior mammogram and projected a white line indicating this boundary onto the breast support as shown in Figure 18. The nipple position was clearly visible and the boundary fitted well to the edge of the phantom, which had not been moved since the prior acquisition, indicating that the projection was a good representation of the positioning in the prior mammogram. The AI based positioning tool was unable to identify the nipple either in the anatomical phantom or in demonstration clinical images. Fujifilm are working to rectify this.

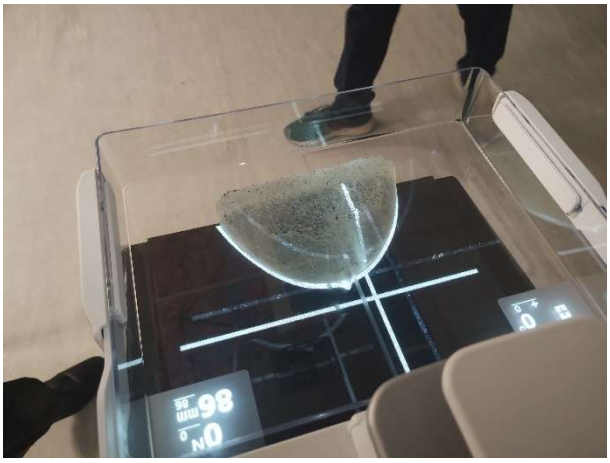

a) The projection from the prior mammogram accurately fits to the phantom.

b) The white cross indicating the nipple position fails to find the nipple

Figure 18. Projection function (positioning MAP)

3.8 Other tests

The results of all the other tests that were carried out were within acceptable limits as prescribed in the NHSBSP protocol [5] and IPEM Report 89 [8].

3.8.1 Alignment

Alignment measurements showed that the light field edge was within 5mm of the edge of the radiation field at the chest wall (IPEM remedial level > 5mm). The radiation field overlapped the edge of the image by up to 4mm (remedial level < 0mm or > 5mm).

3.8.2 Image retention

The image retention factor was 0.07, compared to the NHSBSP upper limit of 0.3.

3.8.3 AEC repeatability

For a series of 5 repeat images, acquired in quick succession, the maximum deviation of mAs from the mean was less than 0.1%. The maximum deviation in SNR from the mean was 1.03%. Sixteen images were acquired at intervals over the full four days of testing. Time points were chosen such that some repeats were in the morning before any other exposure whilst others were immediately after an intensive series of exposures or at the end of the day after a full day of use. The maximum deviation in mAs for these acquisitions was 0.12% - the NHSBSP remedial level is 5%. The maximum deviation in SNR from the mean over the full four days was 1.25%.

3.8.4 Uniformity and artefacts

Uniformity images acquired with PMMA on the breast support in the beam showed a variation in pixel values of 7.6% relative to the central area. The NHSBSP remedial level is 10%. There were no obvious structures or unusual areas within the uniformity images.

With PMMA the sliding ROI method gave a maximum variation from the mean of 7.5% and a maximum variation from the centre of 10.0%. Figure 19 shows the beam profile as a surface plot for an image of the 45mm of PMMA. This shows that the largest non-uniformities are a result of the anode-heel effect.

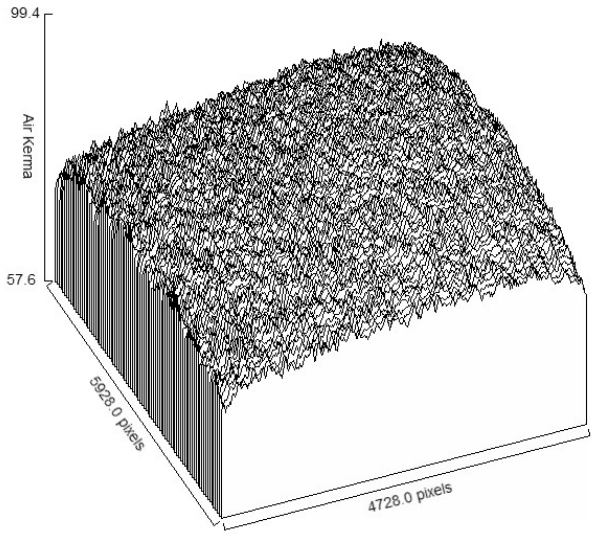

Figure 19. Beam profile of an image of 45mm PMMA under AEC

3.8.5 Cycle time

For a typical exposure of 45mm PMMA using 31kVp W/Rh and 77mAs, a subsequent exposure could be made 5 seconds after the start of the previous one.

3.8.6 Backup timer

When an AEC exposure was attempted with a steel plate blocking the X-ray beam the exposure terminated after the pre-exposure. There was no main exposure and no image acquired.

3.8.7 Focal spot

The measured dimensions of the broad focal spot were 0.57 mm by 0.39 mm - parallel and perpendicular to the chest wall edge respectively – compared to a nominal size of 0.3mm. The focal spot dimensions were just within the maximum permissible values stated in IEC-60336 [22].

3.8.8 Mesh

No significant discontinuities or gaps in signal were visible from the mesh images.

4. Discussion

4.1 Dose and signal difference-to-noise ratio

The detector response was found to be a linear relationship with exposure.

Dance MGDs measured using PMMA were well within the NHSBSP remedial dose levels for all equivalent breast thicknesses when using all AEC dose modes. The Dance MGD to the 53mm thick standard breast model was 1.01mGy in ST mode and 1.45mGy in HQ mode (Table 6). These results are given with iAEC off, as recommended by Fujifilm for phantom exposures, though we found little difference with iAEC on.

SDNR measurements made with plain PMMA showed an overall decrease in SDNR with increased thickness of PMMA (Figure 6). Target SDNR values of 4.1 and 6.0, for minimum acceptable and achievable image quality respectively, were calculated from the SDNR and threshold gold thickness results.

In the ST AEC mode, the SDNRs exceeded the target for the achievable level of image quality for equivalent breast thicknesses of up to 53mm. For higher equivalent breast thicknesses the SDNRs were below the achievable level but above the minimum. In HQ mode the system reached the achievable level up to 60mm equivalent thickness and reached the minimum acceptable level for all thicknesses.

4.2 Local dense area

The local dense area test showed that with segmentation on the AEC identifies the presence of the dense area and increases the mAs in order to maintain SNR and SDNR up to a total tested attenuation of 52mm of PMMA.

4.3 Noise analysis

Noise analysis showed that quantum noise dominates the noise over the whole range of incident air kermas that noise was measured (19 to 311µGy) (Figure 11). The results show that there are minimal contributions from electronic and structural noise.

4.4 Image quality

Threshold gold thicknesses for a range of detail diameters are shown in Figure 12. At an MGD of 1.15mGy (close to that selected for the equivalent thickness of PMMA in Standard mode), the image quality was at or better than the achievable level for all contrast detail diameters.

Threshold gold thickness measurements at different dose levels for the 0.1mm and 0.25mm diameter details were used to calculate Dance MGDs to a 60mm equivalent breast required for the minimum and achievable levels of image quality (Figure 14).

4.5 Quantitative measurements

The quantitative measurements, as indicated by MTF, NNPS and DQE curves (Figure 15, Figure 16, and Figure 17), was provided for reference and was within expected results. The MTF is a typical shape for the Fujifilm system due to the resampling required to change from a hexagonal detector array to a 50μm standard array.

The DQE as defined by the IEC [20] is for the detector alone. These measurements were made within the system and the calculated DQE was affected by the system effects on the MTF and NNPS.

4.6 Projection function (positioning MAP)

The projection function worked well, correctly pulling the prior mammograms for the client and accurately projecting the skin edge onto the detector housing. It was not possible to test how well this worked with priors acquired on other manufacturers systems with different resolutions and pixel sizes. The concept has potential to be useful in breast screening and the philosophy of encouraging thought about positioning at the time is good. We wonder about women who lose or gain weight in the 3 year interval between visits and how such habitus changes might impact the utility of the function.

The AI positioning tool failed to correctly detect the nipple rendering the derived positioning quality scores meaningless. Fujifilm state that the software does not work well with phantoms and that there have been some upgrades to the software since then.

4.7 Comfort comp

The Fujifilm Sophinity offers a novel compression system in which the compression pressure is reduced slightly during the exposure. It is suggested that the breast tissue exhibits a hysteresis effect and largely retains the compressed shape and separation of tissues within the breast during the exposure despite the reduction in pressure. Fujifilm believe that this process does not degrade image quality but provides more comfort for the client. It was not possible to assess these claims by imaging test objects. We suggest that a clinical study comparing the same women imaged with comfort comp on and off is needed before, or possibly as part of, any practical evaluation. Any such study would need to include a range of lesions and we have particular questions about how the appearance of architectural distortions might be affected.

4.8 Other tests

The miscellaneous results presented under the section “Other tests” were mostly satisfactory. The dominant sources of non-uniformity are likely to be the anode-heel effect and scatter distribution. The magnitude of the residual effect in an image is strongly dependent on the density and thickness of the breast (or in this case test object) being imaged. The flat-fielding process therefore doesn’t remove the need for a large-scale gradient correction as part of the image processing before clinical presentation.

5. Conclusions

The technical performance of the Fujifilm Sophinity in 2D mode was found to be satisfactory.

The Dance MGD is well below the remedial level in both the ST and HQ AEC modes. The image quality, as measured by threshold gold thickness, is at the achievable level in ST mode for 60mm equivalent thickness.

6. Acknowledgements

The authors (John Loveland and Alistair Mackenzie) would like to acknowledge the help of Fujifilm staff in providing access to the equipment and for technical support. We also thank Fujifilm for covering the accommodation and meal costs during our visit.

References

[1] A. Mackenzie and J. Oduko, “NHS Breast Screening Programme Equipment Report Technical Evaluation of Hologic 3Dimensions digital mammography system in 2D mode,” Public Health England, London, 2019.

[2] Public Health England, “NHS Breast Screening Programme Equipment Report: Technical evaluation of GE Senographe Pristina digital mammography system in 2D mode,” Public Health England, London, 2019.

[3] C. Strudley, A. Hadjipanteli, J. Oduko and K. Young, “NHS Breast Screening Programme Equipment Report: Technical evaluation of Fujifilm AMULET Innovality digital breast tomosynthesis system,” Public Health England, London, 2018.

[4] J. Loveland and A. Mackenzie, “NHS Breast Screening Programme Equipment Report: Technical Evaluation of Siemens MAMMOMAT B.brilliant digital mammography system in 2D mode,” NHS England, Leeds, 2024.

[5] E. Kulama, A. Burch, I. Castellano, C. Lawinski, N. Marshall and K. Young, “NHSBSP Equipment Report 0604: Commissioning and routine testing of full field digital mammogaphy systems,” NHS Cancer Screening Programmes, Sheffield, 2009.

[6] R. van Engen, S. van Woudenberg, H. Bosmans, K. Young and M. Thijssen, “European guidelines for quality assurance in breast cancer screening and diagnosis (4th edition): European protocol for the quality control of physical and technical aspects of mammgography screening,” European Commission, Luxembourg, 2006.

[7] E. Perry, M. Broeders, C. de Wolf, S. H. R. Törnberg and L. von Karsa, “European guidelines for quality assurance in breast cancer screening and diagnosis - Fourth eddition Supplements,” European Commission, Luxembourg, 2013.

[8] A. C. Moore, D. R. Dance, D. S. Evans, C. P. Lawinski, E. M. Pitcher and A. Rust, “The commissioning and routine testing of mammographic X-ray systems,” Institute of Physics and Engineering in Medicine, York, 2005.

[9] D. R. Dance, “Monte Carlo calculation of conversion factors for the estimation of mean glandular breast dose,” *Physics in Medicine and Biology,* vol. 35, pp. 1211-19, 1990.

[10] D. R. Dance, C. L. Skinner, K. C. Young, J. R. Beckett and J. C. Kotre, “Additional factors for the estimation of mean glandular breast dose using the UK mammography dosimetry protocol,” *Physics in Medicine and Biology,* vol. 45, pp. 3225-40, 2000.

[11] D. R. Dance, K. C. Young and R. E. van Engen, “Further factors for the estimation of mean glandular dose using the United Kingdom, European and IAEA dosimetry protocols,” *Physics in Medicine and Biology,* vol. 54, pp. 4361-72, 2009.

[12] I. Sechopoulos, D. R. Dance, J. M. Boone, H. T. Bosmans, M. Caballo, O. Diaz, R. van Engen, C. Fedon, S. J. Glick, A. M. Hernandez, M. L. Hill, K. W. Hulme, R. Longo, C. Rabin and W. B. Sanderink, “Joint AAPM Task Group 282/EFOMP Working Group Report: Breast dosimetry for standard and contrast-enhanced mammography and breast tomosynthesis,” *Medical Physics,* vol. 51, no. 2, pp. 712-739, 2023.

[13] A. Alsager, K. C. Young and J. M. Oduko, “Impact of heel effect and ROI size on the determination of contrast-to-noise ratio for digital mammography systems,” *International Society for Optics and Photonics, Proc. SPIE 6913 Medical Imaging 2008: Physics of Medical Imaging,* 2008.

[14] A. Hernandez, A. Seibert, A. Nosratieh and J. Boone, “Generation and analysis of clinically relevant breast imaging x-ray spectra,” *Medical Physics,* vol. 44, no. 6, p. 148–2160, 2017.

[15] M. Berger, J. Hubbell, S. Seltzer, J. Chang, J. Coursey, R. Sukumar, D. Zucker and K. Olsen, “XCOM: Photon Cross Sections Database (version 1.5),” November 2010. [Online]. Available: https://www.nist.gov/pml/xcom-photon-cross-sections-database.

[16] R. van Engen, S. Schopphoven, K. Pedersen, N. Marshall, A. Mackenzie, P. Heid, P. Golinelli, M. Chevalier and P. Baldelli, “Quality Control in Digital Breast Tomosynthesis (DBT): EFOMP Protocol 02.2024,” European Federation of Organisations for Medical Physics, Utrecht, 2024.

[17] K. Young, J. Oduko, H. Bosmans, K. Nijs and L. Martinez, “Optimal beam quality selection in digital mammography,” *British Journal of Radiology,* vol. 79, pp. 981-990, 2006.

[18] K. Young, J. Cook and J. Oduko, “Automated and human determination of threshold contrast for digital mammography systems,” *In Proceedings of the 8th International Workshop on Digital Mammography, Berlin: Springer-Verlag,* pp. 4046: 266-272, 2006.

[19] K. Young, A. Alsager, J. Oduko, H. Bosmans, B. Verbrugge, T. Geertse and R. van Engen, “Evaluation of software for reading images of the CDMAM test object to assess digital mammography systems,” *Medical Imaging 2008: Physics of Medical Imaging, Proceedings of the SPIE, Volume 6913, article id. 69131C,,* 2008.

[20] International Electrotechnical Commission, “IEC 62220-1-2: Determination of the detective quantum efficiency – Detectors used in mammography,” International Electrotechnical Commission, Geneva, 2007.

[21] B. Aiazzi, S. Baronti, A. Capanni, L. Santurri and R. Vitulli, “Advantages of hexagonal sampling grids and hexagonal shape detector elements in remote sensing imagers,” in *EUSIPCO'2002 - 11th European Signal Processing Conference*, Toulouse, 2002.

[22] International Electrotechnical Commission, “IEC 60336:2020 - Medical electrical equipment - X-ray tube assemblies for medical diagnosis - Focal spot dimensions and related characteristics,” International Electrotechnical Commission, Geneva, 2020.